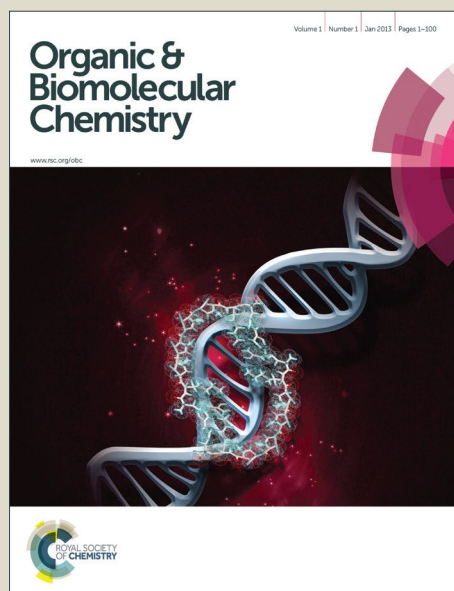


Organic & Biomolecular Chemistry

Accepted Manuscript



This is an *Accepted Manuscript*, which has been through the Royal Society of Chemistry peer review process and has been accepted for publication.

Accepted Manuscripts are published online shortly after acceptance, before technical editing, formatting and proof reading. Using this free service, authors can make their results available to the community, in citable form, before we publish the edited article. We will replace this *Accepted Manuscript* with the edited and formatted *Advance Article* as soon as it is available.

You can find more information about *Accepted Manuscripts* in the [Information for Authors](#).

Please note that technical editing may introduce minor changes to the text and/or graphics, which may alter content. The journal's standard [Terms & Conditions](#) and the [Ethical guidelines](#) still apply. In no event shall the Royal Society of Chemistry be held responsible for any errors or omissions in this *Accepted Manuscript* or any consequences arising from the use of any information it contains.

Benzothiazole hydrazone of furylbenzamides preferentially stabilize *c-MYC* and *c-KIT1* promoter G-quadruplex DNAs

Sushree Prangya Priyadarshinee Pany, Praneeth Bommisetti, K. V. Diveshkumar, and P. I. Pradeepkumar*

Department of Chemistry, Indian Institute of Technology Bombay, Powai,

Mumbai-400076, India

Email: pradeep@chem.iitb.ac.in

Abstract

The stabilization of G-quadruplex DNA structures by using small molecule ligands having simple structural scaffolds has the potential to be harnessed for developing next generation anticancer agents. Because of the structural diversity of G-quadruplexes, it is challenging to design stabilizing ligands, which can specifically bind to a particular quadruplex topology. To address this, herein we report the design and synthesis of three benzothiazole hydrazone of furylbenzamides having different side chains (ligand **1**, **2** and **3**), which show preferential stabilization of promoter quadruplex DNAs (*c-MYC* and *c-KIT1*) having parallel topologies over telomeric and duplex DNAs. CD melting study revealed that all the ligands, in particular ligand **2**, exhibit higher stabilization toward parallel promoter quadruplexes ($\Delta T_m = 10-15$ °C) as compared to antiparallel promoter quadruplex (*h-RAS1*), telomeric quadruplex and duplex DNAs ($\Delta T_m = 0-3$ °C). FID assay and fluorimetric titration results also reveal the preferential binding of ligands toward *c-MYC* and *c-KIT1* promoter quadruplex DNAs over telomeric and duplex DNAs. Validating these results further, *Taq* DNA polymerase stop assay showed $IC_{50} \sim 6.4$ μ M for ligand **2** with *c-MYC* DNA template, whereas the same for telomeric DNA template was found to be > 200 μ M. Molecular modeling and dynamics studies demonstrated 1:1 binding stoichiometry in which stacking and electrostatic interactions play important roles in stabilizing the *c-MYC* G-quadruplex structure. Taken together, the results presented here provide new insights in

the design of structurally simple scaffolds for the preferential stabilization of a particular G-quadruplex topology.

Introduction

G-quadruplexes are the secondary DNA structures formed by the stacking of two or more planar G-quartets in the presence of suitable metal ions such as K^+ and Na^+ .¹⁻³ G-quartets are formed by the H-bond association of adjacent guanine bases by utilizing both Hoogsteen and Watson-Crick faces.² Putative G-quadruplex forming sequences are highly prevalent in the human genome and they are mostly present at the telomere, gene promoters, introns and at the immunoglobulin switch regions.^{4,5} Recently, *in vivo* existence of G-quadruplex structures has been visualized by immunofluorescence staining using structure specific BG4 antibodies as well as fluorescent light up probes.⁶⁻⁸ The G-quadruplex structures can adopt various topologies and their structural polymorphism depend on the strand orientation, size/sequence of the loops, glycosidic torsional angles and nature of the metal ions present in the medium.⁹ For the human telomeric G-quadruplex DNA, various conformations such as antiparallel, (3+1) hybrid and parallel topologies are observed under different metal ion and molecular crowding conditions.¹⁰ G-quadruplex structures formed at the promoter regions are well characterized to adopt mostly parallel topology under K^+ conditions.^{11,12}

G-quadruplex structures present in the telomeric and promoter regions were explored for their roles in telomerase inhibition and regulation of gene expression, respectively, in the past few decades.¹³⁻¹⁵ Therefore, stabilization of these quadruplex structures by using small molecule ligands has emerged as an attractive area in the anticancer drug development.¹⁶⁻¹⁹ Most of the reported ligands provide a planar aromatic surface for π -stacking interaction with the external surface of the G-quartet. Along with this, recognition was also provided by the electrostatic as well as H-bonding interactions of neutral/cationic side chain with the loops/grooves and phosphate backbone of the quadruplex structure.²⁰ A wide range of G-quadruplex stabilizing ligands such as telomestatin,²¹ diarylethynylamides²², naphthyridine derivatives,²³ DPC derivatives,²⁴ xanthene and xanthone derivatives²⁵ were

reported for their selective stabilization toward G-quadruplex over duplex DNAs. Piperazinylquinoline derivatives,²⁶ ellipticine derivatives,²⁷ *N*-substituted berberine derivatives,²⁸ bisaryldiketene derivatives²⁹ and furan based cyclic homoligopeptides³⁰ were reported for selective stabilization of *c-MYC* quadruplex over duplex DNAs and down regulation of *c-MYC* gene expression. Though these ligands selectively stabilize G-quadruplex over duplex DNA, most of them fail to achieve specificity or preference toward a particular G-quadruplex topology. Therefore, it is highly challenging to design ligands in a structure specific fashion to discriminate different quadruplex topologies. Such ligands may be desirable to achieve target specific therapeutic impact in malignant cells. The structure specific ligands should be designed by utilizing unique recognition elements of the loops and grooves of the quadruplex along with the recognition of varying dimensions of G-quartets.¹⁹ There are only handful of topology specific ligands reported in the literature. Our group has recently reported indenopyrimidine derivatives,³¹ and bisbenzimidazole carboxamide derivatives,³² which show specific stabilization of parallel topology of promoter over telomeric G-quadruplex and duplex DNAs. Pyridyl peptidomimetic ligands have been reported for their specific stabilization toward *c-KIT1* DNA over other quadruplex and duplex DNAs.³³ Recently, disubstituted benzofuran derivatives have been identified using a small molecule micro array screens as specific inhibitor for *c-MYC* gene expression.³⁴

In our continued efforts to develop topology specific G-quadruplex stabilizing ligands having simple structural scaffolds harbouring drug-like-properties, herein, we report a new series of ligands based on benzothiazole hydrazone moiety coupled with furylbenzamide group anchoring different side chains (Figure 1). The binding interaction, stability and selectivity of these ligands toward G-quadruplex (*c-MYC*, *c-KIT1*, *h-RAS1* and telomeric) and duplex DNAs have been explored by various biophysical and biochemical methods such as CD titration, CD melting, fluorescence intercalator displacement (FID) assay and *Taq* DNA

polymerase stop assay. The results show that these ligands preferentially stabilize the parallel topology of *c-MYC* and *c-KIT1* promoter quadruplex DNAs over antiparallel topology of *h-RAS1* promoter DNA, various topologies of telomeric quadruplex and duplex DNAs. The binding mode and interaction between the ligand and quadruplex DNA were explored by harnessing molecular modeling and dynamics studies.

Results and discussion

Ligand design and synthesis. Benzothiazole moieties are considered as one of the foremost building blocks in medicinal chemistry due to their prevailing biological relevance.³⁵ These entities show a very wide range of biological activities including cytotoxicity against tumorigenic cell lines.³⁶ Arylfuran groups are reported for their antiproliferative activity in human leukemia cells.^{37,38} Recently, a series of compounds containing furyl-benzothiazole hydrazone derivatives are reported for their selective inhibition of *BCL-X_L* protein.³⁹ This widely explored biological applications inspired us to utilize such a heteroaromatic core, which can be turned as G-quadruplex stabilizing ligands. Owing to the structural similarity of benzothiazoles with guanine base of

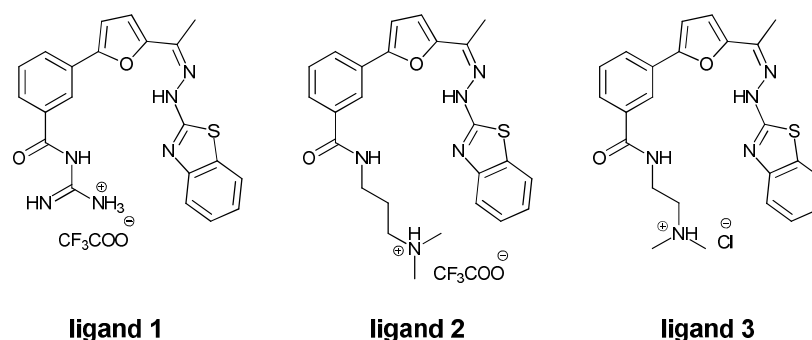
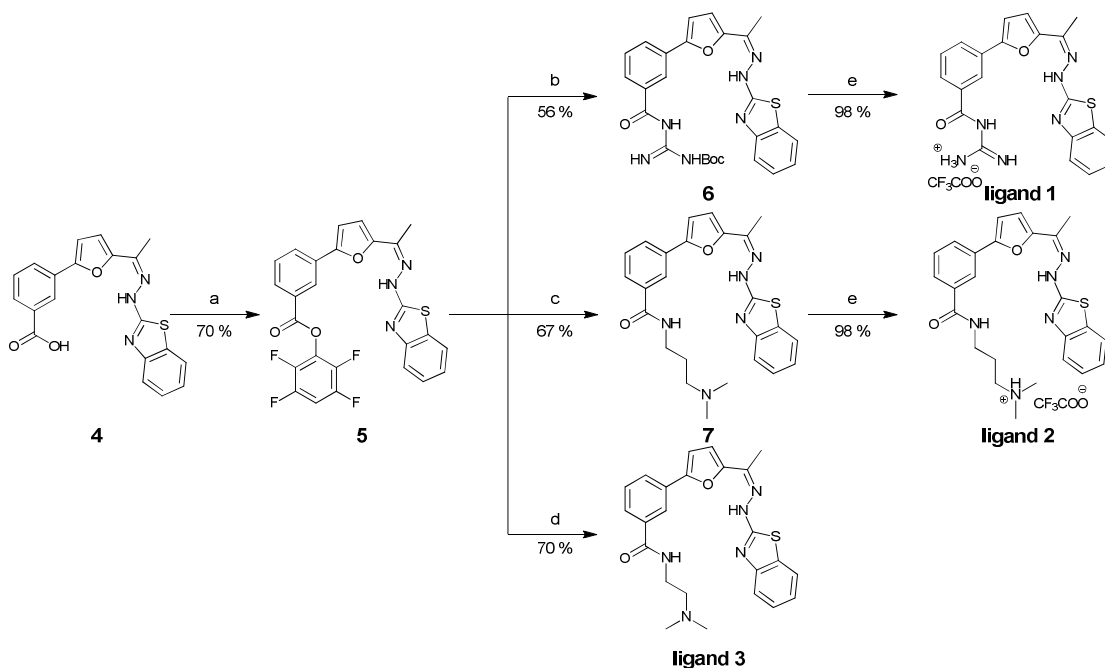


Figure 1. Structure of G-quadruplex stabilizing ligands based on benzothiazole hydrazone of furylbenzamide scaffolds

G-quartets, they are expected to provide the stacking interaction with the G-quartets. Thus, we envisioned that incorporation of suitable side chains such as benzamides into the furyl-benzothiazole hydrazone scaffold can enhance the recognition and stabilization properties of

the ligands. To achieve this, we have designed three ligands having a common aromatic core with guanidinium, ethyl and propyl side chains (Figure 1). These positively charged side chains of varying nature and lengths were exploited to discriminate between topologically different loops and grooves present in the quadruplex structures.



Scheme 1. Synthesis of ligand **1**, **2** and **3**. Reagents and conditions: a) EDCI, 2,3,5,6-tetrafluorophenol, DMF, RT, 6 h; b) *N*-Boc-guanidine, DCM:MeOH (1:1), RT, 3 h; c) *N,N*-dimethylpropane-1,3-diamine, DCM, RT, 3 h; d) *N,N*-dimethylethane-1,2-diamine, DCM, RT, 3 h; e) Trifluoroacetic acid, DCM, RT, 1 h.

Synthetic route utilized to access all the three ligands is depicted in Scheme 1. Synthesis was embarked from compound **4**, which was prepared by following a previously reported procedure.³⁹ Surprisingly, the direct amide coupling of **4** with the side chains employing different coupling agents such as EDCI, HATU and BOP yielded products along with inseparable impurities. This forced us to employ a two-step procedure.⁴⁰ First, the compound **4** was converted 2,3,5,6-tetrafluoro phenolic ester **5** in 70% yield. Further, the ester **5** was converted to various amides **6**, **7** and **3** using the corresponding amines in 56%, 67% and 70% yields respectively. Finally, the amides **6** and **7** were treated with trifluoroacetic acid to furnish the protonated ligands **1** and **2**. However, we found that

purification of trifluoroacetate salt of **3** was cumbersome, and therefore a stock solution of the same in 10 mM HCl was prepared for various biophysical and biochemical studies.

Circular dichroism titration studies. Various topologies of G-quadruplex DNA structures can be qualitatively characterized by using circular dichroism (CD) spectroscopy.⁴¹ CD titration spectra of telomeric DNA in the absence of any added metal ions showed two positive bands: one dominant at 254 nm and a small band around 290 nm, which are not attributed to any specific quadruplex topologies. Upon titration of telomeric DNA with ligand **1**, peak intensity at 290 nm was increased moderately, whereas with ligand **2** and **3**, a less increment was observed in a concentration dependant manner (Figure 2A, Figure S1, Supporting Information). Also, a new negative band at 260 nm with moderate intensity gradually started appearing along with the shifting of the peak from 254 nm to 244 nm (Figure 2A, Figure S1, Supporting Information). These moderate enhancement of ellipticities at 290, 260 and 244 nm indicate the weak induction of antiparallel topology for the telomeric quadruplex DNA by the ligands.

Unlike telomeric quadruplex DNA, most of the promoter G-quadruplex DNAs are reported to exhibit parallel topology even in the absence of any added monovalent metal ions.²² The CD spectra for both *c-MYC* and *c-KIT1* DNAs without any added monovalent metal ions was found to have a positive peak at 260 nm and a negative peak at 240 nm, which reveals the preformed parallel topologies of these quadruplex DNAs (Figure 2B, Figure S1 and S2, Supporting Information). For the *c-MYC* DNA, peak ellipticity at both 260 and 240 nm was found to be linearly increasing with the ligand concentration and attains saturation after the addition of 4 equivalents of ligands (Figure 2B, Figure S1, Supporting Information). Dramatic increase in the intensity of the characteristic peaks signifies further stabilization of pre-folded

parallel G-quadruplex topology for the *c-MYC* quadruplex DNA by all the ligands. Similarly, titration studies were performed with *c-KIT1* quadruplex DNAs and moderate stabilization of the existing parallel topology was observed with all the three ligands (Figure S2, Supporting Information).

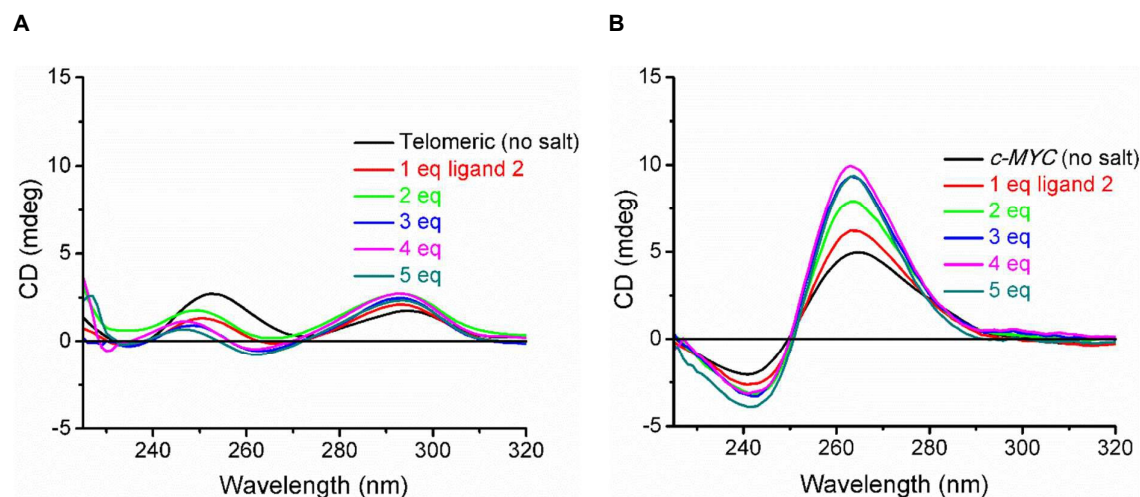


Figure 2. CD titration spectra of telomeric and *c-MYC* DNAs (12.5 μ M in 50 mM Tris-HCl, pH 7.2). (A) Telomeric DNA; and (B) *c-MYC* DNA with increasing concentration of ligand **2** (0-5equiv) in the absence of added monovalent metal ions.

Moderate induction of antiparallel topology for telomeric DNA by the ligands prompted us to investigate whether the ligands are able to stabilize antiparallel topology of *h-RAS1* promoter DNA reported under K^+ ions.⁴² The molar ellipticity of *h-RAS1* DNA without any added monovalent metal ion showed a positive peak at 280 nm and a negative peak at 246 nm, which does not account for any particular quadruplex topology. The addition of up to 6 equivalents of ligand **2** could not induce any particular quadruplex topology to this DNA (Figure S2, Supporting Information). Overall, the observations from CD titration studies suggest that the ligands are able to weakly induce antiparallel topology of telomeric G-quadruplex DNA and can further stabilise the parallel topology of *c-MYC* and *c-KIT1* promoter quadruplex DNAs. Nevertheless, the ligand fail to induce or stabilize antiparallel topology of *h-RAS-1* promoter DNA.

CD melting studies. CD melting experiments were carried out to assess the thermal stabilization properties of ligands with various G-quadruplex and duplex DNAs by following reported experimental procedures.⁴³ Thermal stabilization of telomeric DNA as well as promoter and duplex DNAs were studied by monitoring at respective wavelength of maximum intensities in the CD spectra. Melting experiments for telomeric DNA was recorded at 295 nm under K^+ conditions (10 mM) which yielded a melting temperature of 53 °C (Figure 3A). After the addition of 5 equivalents of ligands, there was no considerable increase in the melting temperature with any of the three ligands (Table 1). Since the ligands were shown to weakly induce antiparallel topology of the telomeric DNA, we examined the stabilization effect of ligands toward the antiparallel telomeric DNA structure by performing the melting experiment in presence of Na^+ ions (30 mM).⁴⁴ The molar ellipticity of telomeric DNA was monitored at 295 nm to provide melting temperatures of 45 °C. Addition of 5 equivalents of ligands resulted only in weak stabilization of the antiparallel topology ($\Delta T_m \sim 2.5$ -3 °C) (Table 1 and Figure S3, Supporting Information).

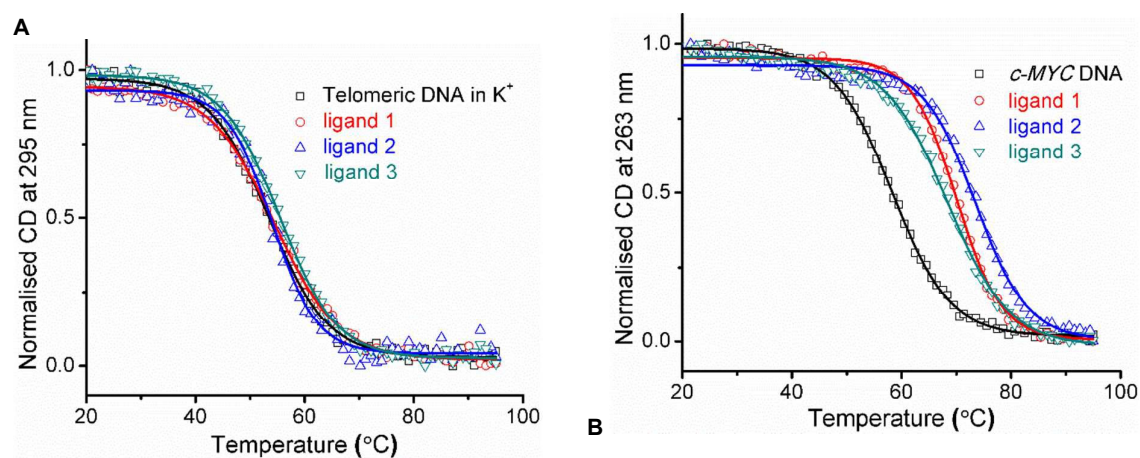


Figure 3. Normalised CD melting curve of telomeric and *c-MYC* quadruplex DNAs (10 μ M in 10 mM lithium cacodylate buffer, pH 7.2) in the absence and presence of 5 equivalents of ligands. (A) Telomeric DNA (10 mM KCl and 90 mM LiCl); and (B) *c-MYC* DNA (1 mM KCl and 99 mM LiCl)

For parallel promoter G-quadruplex DNAs (*c-MYC* and *c-KIT1*), the melting temperatures (T_m) were monitored at 263 nm under K^+ ions and high enhancement of thermal

stabilizations were observed after the addition of ligands (Figure 3B and Figure S3, Supporting Information). Addition of ligand **2** to *c-MYC* and *c-KIT1* quadruplex DNAs furnished an increase in melting temperature of 15.3 °C, whereas ligands **1** and **3** showed slightly less enhancement in melting temperatures ($\Delta T_m \sim 10\text{--}13.5$ °C) (Table 1, Figure 3B and Figure S3, Supporting Information). Additionally, the thermal stabilization effect of ligands on the antiparallel *h-RAS1* promoter DNA was investigated by monitoring the CD signal at 290 nm under K^+ ions (50 mM). The addition of 5 equivalents of ligands provided a modest increase in melting temperature (maximum $\Delta T_m \sim 2.5$ °C) suggesting very weak stabilization of this particular antiparallel topology (Table 1 and Figure S3, Supporting Information). These results clearly show that ligand **2** with propyl side chain is more efficient in achieving preferential stabilization of parallel topologies of *c-MYC* and *c-KIT1* quadruplex DNAs.

Table 1. Thermal stabilization of various quadruplex and duplex DNAs determined from CD melting experiments.

Ligands	$^a\Delta T_m$					
	Telomeric (K^+)	Telomeric (Na^+)	<i>c-MYC</i>	<i>c-KIT1</i>	<i>h-RAS1</i>	Duplex (ds 17)
1	1.2 ± 0.1	3.0 ± 0.1	11.8 ± 0.2	13.5 ± 0.9	2.3 ± 0.1	-0.5 ± 0.1
2	0.6 ± 0.1	2.5 ± 0	15.3 ± 0.2	15.3 ± 0.5	1.3 ± 0.1	-1.3 ± 0.1
3	1.7 ± 0.1	3.0 ± 0.2	10 ± 0.2	11.3 ± 0.5	2.4 ± 0.1	-1.0 ± 0.1

$^a\Delta T_m$ stands for the difference in the thermal melting [$\Delta T_m = T_m$ (DNA + 5 molar equivalent ligand) – T_m (DNA)]. The reported values are the average of three independent experiments with estimated standard deviations. All the experiments were carried out using 10 μ M quadruplex DNA or 15 μ M duplex DNA in 10mM lithium cacodylate buffer, pH 7.2 for telomeric (K^+) and promoter DNAs or in 10 mM sodium cacodylate buffer, pH 7.2 for telomeric DNA (Na^+). The T_m values in the absence of ligands are 53.2 ± 0.2 for telomeric DNA in the presence of K^+ ion (10 mM KCl and 90 mM LiCl), 45.1 ± 0.5 for telomeric DNA in the presence of Na^+ ion (20 mM NaCl and 80 mM LiCl), 57.8 ± 0.4 for *c-MYC* DNA (1 mM KCl and 99 mM LiCl), 46.6 ± 0.6 for *c-KIT1* DNA (10 mM KCl and 90 mM LiCl), 53.8 ± 0.4 for *h-RAS1* DNA (50 mM KCl and 50 mM LiCl) and 64.0 ± 0.2 for ds 17 DNA (10 mM KCl and 90 mM LiCl).

To further investigate the selectivity of ligands toward G-quadruplex DNA over duplex DNAs, melting experiments were performed at 242 nm with the duplex DNA. The stabilizing effect of the ligands on duplex DNA was found negligible (Table 1 and Figure S3, Supporting Information). Overall, results from CD melting studies reveal that all the three ligands preferentially stabilize the parallel topology of promoter quadruplex (*c-MYC* and *c-KIT1*) over the telomeric quadruplex and duplex DNAs. Moreover, ligand **2** was found to be more potent in preferentially stabilizing the parallel promoter quadruplex DNAs when compared to the other two ligands.

Fluorescence intercalator displacement (FID) assay. To support the findings from the CD titration and melting results, FID assay was performed. FID assay is based on the efficiency of the ligands to displace thiazole orange (TO) from its complex with quadruplex DNA, and the percentage of displacement can be plotted against the concentration of ligand to afford the DC_{50} values.⁴⁵ Low DC_{50} values represent the high binding affinity of the ligand toward quadruplex

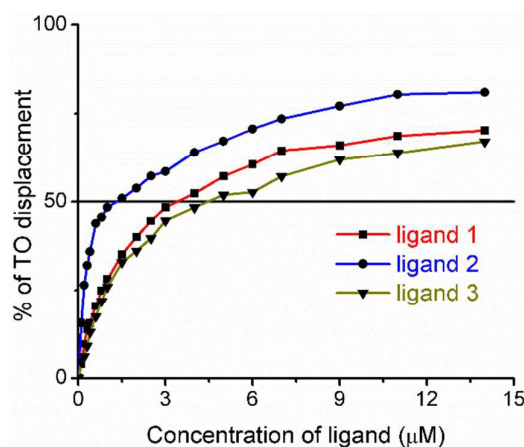


Figure 4. Plot of percentage of TO displacement from *c-MYC* quadruplex DNA by the ligands **1**, **2**, and **3**. FID titrations were carried out by using 0.25 μM DNA and 0.5 μM TO in buffer (100 mM KCl, 10 mM lithium cacodylate, pH 7.2). Ligand concentrations were varied from 0-14 μM .

DNA. For the *c-MYC* DNA, all the three ligands were able to furnish low DC_{50} values (1.31-4.4 μM), indicating high stabilization of *c-MYC* quadruplex DNAs by the ligands (Table 2

and Figure 4). Similarly, in the case of *c-KIT1* quadruplex DNA moderate DC_{50} (5.5-7.5 μM) values were observed for all the three ligands (Table 2 and Figure S4, Supporting Information). However, for telomeric quadruplex DNA and duplex DNAs, high DC_{50} values ($\sim 15 \mu\text{M}$ to $27 \mu\text{M}$) were obtained from FID studies. These results clearly indicate that the ligands are not able to strongly stabilize telomeric and duplex DNAs (Table 2 and Figure S4, Supporting Information). For *c-MYC* and *c-KIT1* DNAs as observed from the CD melting experiments,

Table 2. DC_{50} values for telomeric, *c-MYC*, *c-KIT1* and duplex DNAs with all three ligands measured from FID assay

Ligands	TO displacement (DC_{50} in μM) ^a			
	Telomeric (K^+)	<i>c-MYC</i>	<i>c-KIT1</i>	Duplex (ds 17)
1	15.5 ± 0.5	3.36 ± 0.2	5.6 ± 0.1	17.6 ± 0.6
2	26.7 ± 0.1	1.31 ± 0.1	3.5 ± 0.2	25 ± 0.5
3	16.4 ± 0.3	4.43 ± 0.5	7.55 ± 0.9	21.3 ± 0.7

^a DC_{50} denotes the concentration of ligands required to displace 50 % of TO. All the experiments were triplicated and the values are shown with estimated standard deviations. For all the experiments, 0.25 μM DNA in 100 mM KCl and 10 mM lithium cacodylate buffer, pH 7.2 were used with incubation (2 h) of 2 equivalent of TO for quadruplex DNAs and 3 equivalent of TO for duplex DNA.

ligand **2** with the propyl side chain, was found to be more potent with lowest DC_{50} value compared to the other two ligands. In addition to that, all the three ligands showed slight preference toward the *c-MYC* over the *c-KIT1* quadruplex DNA.

Fluorimetric titration studies. To explore preferential binding of ligands toward various quadruplex and duplex DNAs, fluorescence titration experiments were performed with ligand **2**, which was evolved as the most effective quadruplex stabilizer. Ligand **2** showed an absorption maximum at 367 nm and strong fluorescence emission around 450 nm. Increasing concentration of ligand (0-50 μM) was titrated against fixed concentration of pre-annealed DNAs (5 μM) and emission spectra were recorded. Upon addition of ligand **2** to *c-MYC* quadruplex DNA, ~ 60 fold enhancement of fluorescence intensity was observed in a

concentration dependent manner and saturation was attained at $\sim 24 \mu\text{M}$ ligand concentration (Figure 5A). But, in the case of telomeric quadruplex DNAs similar enhancement of fluorescence intensity was attained at a ligand concentration of $50 \mu\text{M}$ (Figure S5, Supporting Information). As expected, titration of ligand **2** with duplex DNA yielded negligible (~ 10 fold) enhancement in the fluorescence intensity at $50 \mu\text{M}$ saturation concentration. (Figure S5, Supporting Information). Binding constant was deduced by plotting normalised fluorescence intensity against the logarithm of concentration of ligand and was fitted by using Hill1 equation.^{46,47} The apparent binding constant (K_a) of ligand **2** with *c-MYC* quadruplex DNA was found to be $(1.3 \pm 0.3) \times 10^5 \text{ M}^{-1}$ (Figure 5B). Binding constants with telomeric quadruplex DNA and duplex DNA were found to be $(7 \pm 0.1) \times 10^4$ and $(2.7 \pm 0.1) \times 10^4 \text{ M}^{-1}$ respectively (Figure S5, Supporting Information). The apparent K_a values emerged from the fluorimetric

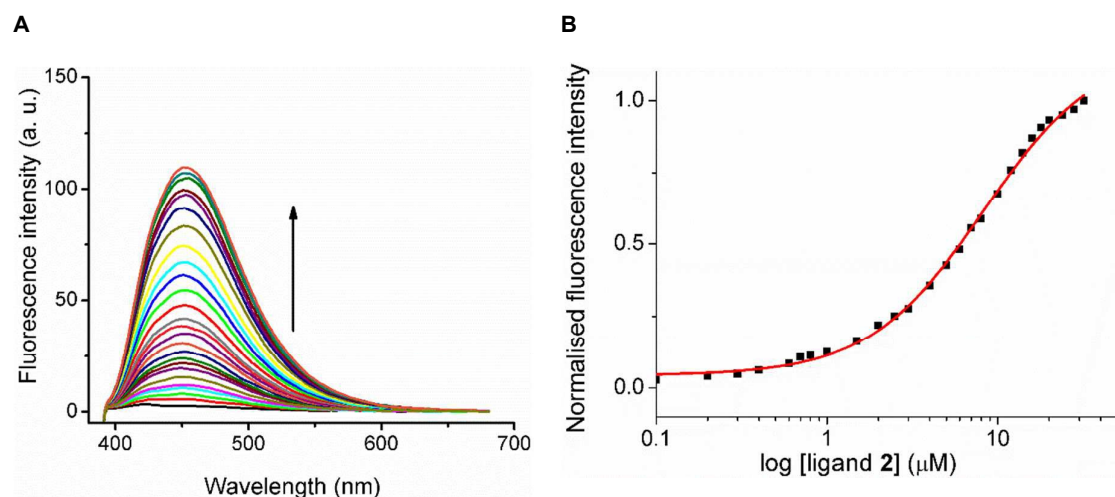


Figure 5. (A) Emission spectra of ligand **2** complexed with *c-MYC* quadruplex DNA [$5 \mu\text{M}$ in 100 mM KCl and 10 mM lithium cacodylate, $\text{pH } 7.2$ with increasing concentration of ligand **2** (0 – $24 \mu\text{M}$)] and (B) Plot of normalised fluorescence intensity against the logarithm of increasing concentration of ligand **2**. Hill1 equation was used for curve fitting.

titration suggest that there is only two and five fold preference for the ligand binding to *c-MYC* quadruplex over telomeric and duplex DNAs respectively. It should be noted here that irrespective of the moderate binding preference, ligands show strong stabilization of the

parallel topologies of *c-MYC* and *c-KIT1* promoters, which was revealed in the CD melting, FID and *Taq* polymerase stop assays (see below).

***Taq* DNA polymerase stop assay.** Having established the preferential stabilization and binding of ligands toward the *c-MYC* and the *c-KIT1* structures, we further investigated the quadruplex targeting efficiency of ligands with the aid of *Taq* DNA polymerase stop assay.^{48,49} Experiments were performed with templates containing *c-MYC* and mutated *c-MYC* DNAs at 55 °C and with telomeric DNA at 40 °C. For the *c-MYC* DNA, there was a concentration dependant increase in the formation of stop products with all the three ligands

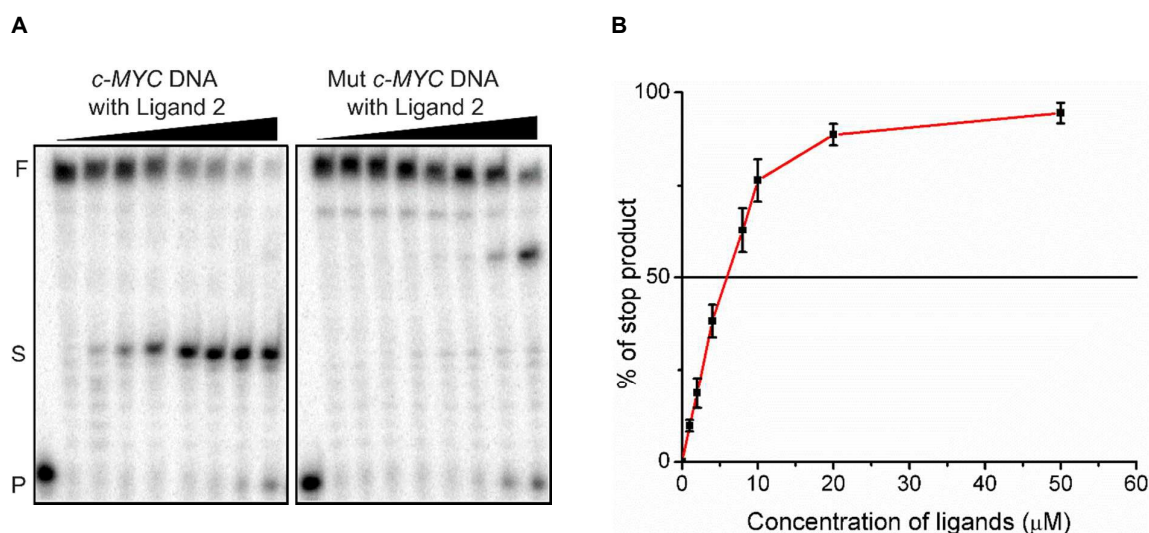


Figure 6. (A) 15% denaturing PAGE (7 M Urea) of *Taq* DNA polymerase stop assay of *c-MYC* DNA template with increasing concentration of ligand **2** (0-50 μM) and of mutated *c-MYC* DNA template with ligand **2** (0-200 μM); and (B) Plot of percentage of stop product against the increasing concentration of ligand **2**. Conditions: 100 nM template DNA, 50 nM primer, 0.2 mM dNTPs and 0.5 U *Taq* DNA polymerase enzyme in buffer (50 mM Tris-HCl, pH 7.2, 0.5 mM DTT, 0.1 mM EDTA, 5 mM MgCl₂, 5m M KCl). P, S and F denote primer, stop product and full length product respectively.

(Figure 6A and Figure S6, Supporting Information). Among the three ligands, ligand **2** showed the lowest IC₅₀ value of ~ 6.4 μM indicating higher stabilization of the *c-MYC* quadruplex DNA whereas, ligand **1** and ligand **3** showed moderate to high IC₅₀ values (~ 14 and ~ 37 μM respectively) (Figure 6B and Figure S7, Supporting Information). As expected,

there were no stop products observed for mutated *c-MYC* DNA under similar reaction conditions and ligand concentrations (Figure 6A and Figure S6, Supporting Information).

Furthermore, stop assay with template containing telomeric DNA yielded very high IC_{50} values for ligand **1** and **3** ($\sim 140 \mu M$ and $\sim 145 \mu M$ respectively) and there was only 16% stop products observed for ligand **2** even at $200 \mu M$ (Figure S6, Supporting Information). These results show that all the three ligands are able to possess preferential stabilization toward the *c-MYC* promoter quadruplex over the telomeric quadruplex DNA. Moreover, the findings from stop assay are in good agreement with the outcomes from the biophysical studies, and the ligand **2** is found to be more efficient toward the preferential stabilization of *c-MYC* promoter quadruplex structure.

Molecular modeling and dynamics study. To elucidate the mode of binding and the major factors governing the G-quadruplex recognition, molecular modeling and dynamics studies were carried out using ligand **2** and *c-MYC* and *c-KIT1* structures. The energy optimized ligand **2** at HF/6-311G** level having *syn* conformation (Figure S8, Supporting Information) was docked with *c-MYC* (PDB entry: 2L7V)⁵⁰ and *c-KIT1* (PDB entry: 2O3M)⁵¹ DNAs using AutoDock 4.2.⁵² While the whole DNA was considered in case of docking with *c-MYC*, a restricted grid docking was carried out at the 5' end of *c-KIT1*. The docking revealed the formation of 1:1 ligand-G-quadruplex complexes for both *c-MYC* and *c-KIT1*. The results show that the ligand **2** preferably stacks at the 5' end of *c-MYC* with nitrogen atom on the propyl side chain involved in electrostatic interactions with the backbone phosphate atoms. And with *c-KIT1*, it was observed that the furan and benzene rings of the ligand **2** stacks over the G-quartet core with the protonated nitrogen atom on the propyl side chain of the ligand involved in electrostatic interactions with the backbone phosphate atoms. Based on the docking results, a total of 500 ns unrestrained molecular dynamics (MD) simulations were performed with the complexes using PMEMD in AMBER 14.⁵³⁻⁵⁶

To verify the conformational stability of the complexes during the course of dynamics, the root mean square deviation (RMSD) values of the heavy atoms of the ligand **2**, DNA backbone, and the G-quartets with respect to the first frame were calculated for each of the complexes. The RMSD values (Figure 7) of the G-quartets showed minimal fluctuations and suggest that the ligand **2** stabilizes the G-quadruplexes. However, the backbone RMSD values fluctuate because of flanking and loop nucleotides. This is evident from the high root mean square fluctuation (RMSF) values of loop and flanking nucleotides compared to those of the guanines in the G-quartets (Figure S9, Supporting Information). The ligand RMSD values

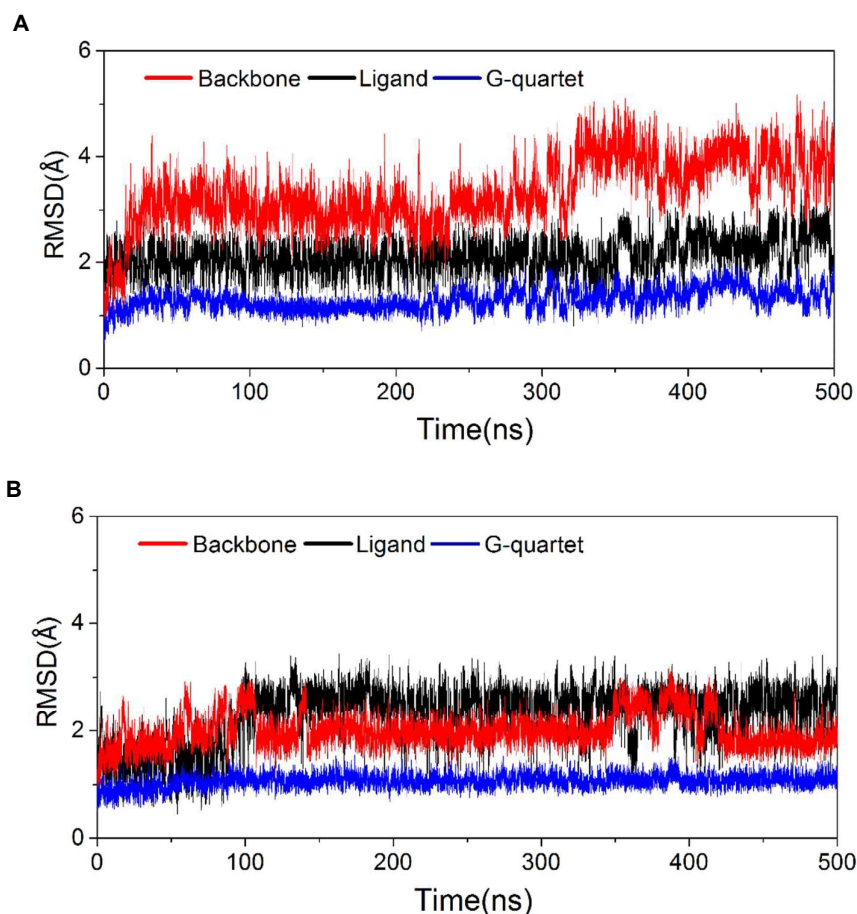


Figure 7. Time dependent root mean square deviation (RMSD) graphs of (A) ligand **2** bound *c-MYC* complex; and (B) ligand **2** bound *c-KIT1* complex. RMSDs of backbone (red), ligand (black) and G-quartet core (blue) are plotted against time. Only heavy atoms of ligand were considered while

calculating RMSD values. G-quartet core include top, middle and bottom G-quartets and backbone atoms include C3',O3',C5',O5', P,OP1 and OP2.

fluctuate to some extent owing to the dynamic nature of propyl side chain. The percentage occupancies of Hoogsteen H-bonds for the G-quartets were calculated and found to be > 96% for both *c-MYC* and *c-KIT1* complexes (Figure S10 and S11, Supporting Information). In the case of both the complexes, the top quartets (5'-end) where the ligand stacks showed > 99% H-bond occupancies. This implies that the top G-quartets are being strongly stabilized by the ligand **2**.

During the course of dynamics with the *c-MYC* DNA, ligand **2** undergoes a rigorous reorientation (Figure S12, Supporting Information). Before starting the production run, the ligand completely stacks over the top G-quartet, but at a time frame of 380-400 ns, the ligand is slightly displaced by the flanking residue dA3, which in turn stacks on the G-quartet (Figure S13A, Supporting Information). During this time, only the furan ring of the ligand **2** exhibited stacking interactions with the G-quartet. The final MD snapshots are shown in Figure 8, which clearly show that eventually the ligand **2** replaces dA3 and the whole ligand stacks over the G-quartet core (Figure 8C). Overall, the stacking interactions have been found to be crucial in stabilizing the ligand-*c-MYC* complex. The parameters, which contribute to stacking from each of the rings of ligand **2** are summarized in Table S1. The stacking contribution from the benzothiazole ring of the ligand **2** was observed to be maximum followed by benzene ring and furan ring. To unravel the electrostatic interactions, the distance between the protonated nitrogen atom on the propyl side chain of the ligand **2** and the phosphate atoms of the *c-MYC* backbone was probed. The major interactions observed were with OP2 atom of residue dG8 with an average distance of 2.9 ± 0.2 Å, and OP1 atom of residue dG13 with an average distance of 2.8 ± 0.2 Å (Figure S14A and S14B, Supporting Information). Also, an ion-induced dipole interaction was observed between the nitrogen atom on the propyl side chain of the ligand and O6 atom of the flanking residue dG2 for a

very brief amount of simulation time ($\sim 4\text{-}5\%$) with an average distance of $3.0 \pm 0.2 \text{ \AA}$ (Figure S14C, Supporting Information). Overall, these electrostatic interactions were observed for $\sim 12\text{-}15\%$ of simulation time (Figure S15, Supporting Information).

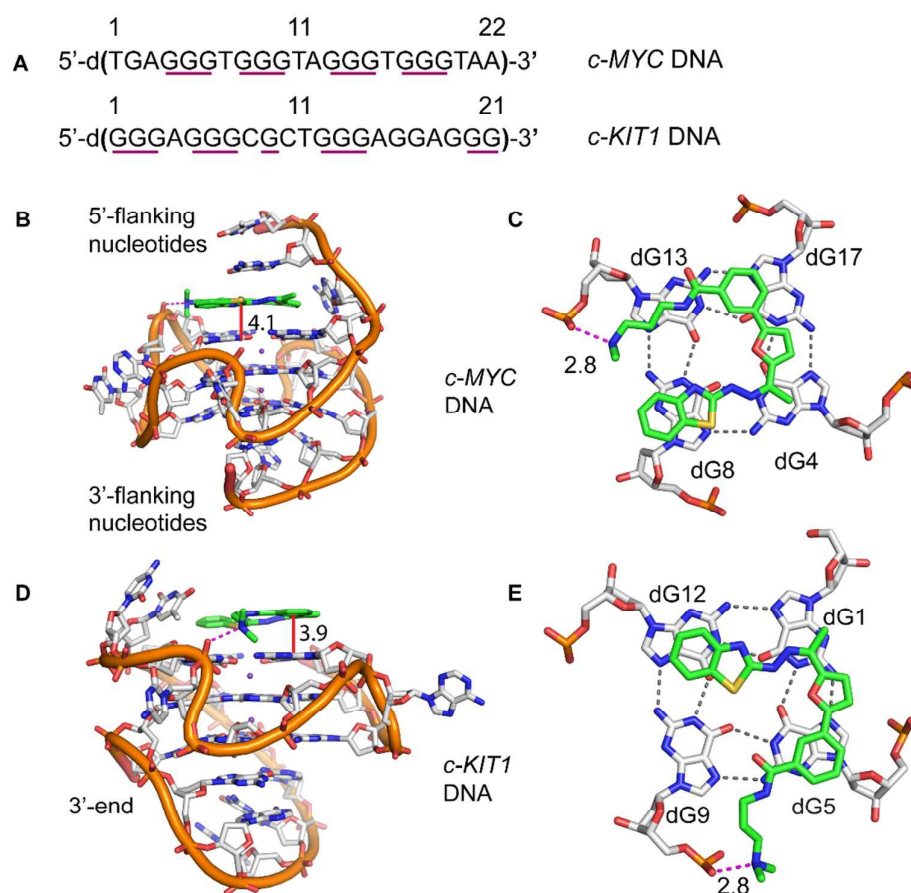


Figure 8. Sequences of *c-MYC* and *c-KIT1* DNAs and averaged MD snapshots of ligand **2** bound *c-MYC* and *c-KIT1* from last 2 ns of 500 ns simulations. (A) Sequences of *c-MYC* and *c-KIT1* DNAs used for modeling studies; (B) Ligand **2** bound to 5'-end face of *c-MYC* DNA (side view); (C) Axial view of stacked ligand **2** with *c-MYC* DNA showing electrostatic interactions; (D) Ligand **2** bound to the 5'-end face of *c-KIT1* DNA; and (E) Axial view of stacked ligand **2** with *c-KIT1* DNA showing electrostatic interactions. The red lines in A and B indicate the average distance between nucleobases and ligand. The dashed magenta lines represent the electrostatic interactions. The K^+ ions are shown as purple spheres. G-quartet forming sequences are underlined in purple. Distances are mentioned in \AA .

It was also observed that the ligand undergoes reorientation during the course of dynamics with the *c-KIT1* DNA but less significantly compared to *c-MYC* DNA (Figure 8B and Figure S16, Supporting Information). Results show that the benzothiazole ring of the

ligand **2** is the major contributor for the stacking with G-quartet followed by the benzene ring (Table S1). As seen from Figure 8E, the benzothiazole ring of the ligand stacks over the dG12 residue, and benzene ring on the dG5 residue. Electrostatic interactions also play a major role in stabilizing the ligand-*c-KIT1* complex.

The protonated nitrogen atom on the propyl side chain of the ligand **2** makes electrostatic contacts with the phosphate atom of residue dG9 with an average distance of 2.8 ± 0.1 Å (Figure S17A, Supporting Information). This interaction was present for $\sim 45\%$ of the simulation time (Figure S18, Supporting Information), and was more predominant toward the end of dynamics. An ion-induced dipole interaction between nitrogen atom on the propyl side chain of the ligand **2** and O2 of dC10 (Figure S17B, Supporting Information) was also observed but for a very brief amount of simulation time ($\sim 4\text{-}5\%$) with an average distance of 3.0 ± 0.2 Å. The loop residues dC10, dT11 were found to be far away from the G-quartet core at the start of dynamics, but toward the end of dynamics, the residue dT11 tends to stack over the benzothiazole ring of the ligand **2**, while the residue dC10 stacks well on dT11 (Figure S13B, Supporting Information). Overall, the results reveal that stacking and electrostatic interactions play a major role in the stabilization of the *c-KIT1* G-quadruplex-ligand **2** complex. There were no prominent intermolecular H-bonds observed between ligand and DNA in both the complexes.

Table 3. Binding free energy components of ligand **2**-quadruplex complexes.

DNA	ΔH	$T\Delta S$	$\Delta G(\Delta H - T\Delta S)$
<i>c-MYC</i> (2L7V)	-48.8 ± 4.2	-17.6 ± 5.1	-31.2 ± 6.7
<i>c-KIT1</i> (2O3M)	-35.6 ± 4.1	-17.6 ± 4.3	-18.0 ± 6.0

Enthalpy values are calculated using MM-PBSA method and entropy values were obtained through nmode calculations. All values are in kcal mol⁻¹.

Binding free energies (ΔG) for both G-quadruplex-ligand complexes were estimated using the MM-PBSA method.⁵⁷ The free energy components are summarized in Table 3 and Table S2. The binding free energy of ligand **2** with *c-KIT1* was -18.02 ± 6.00 kcal mol⁻¹ and that with *c-MYC* was -31.18 ± 6.74 kcal mol⁻¹. Since the entropy loss of the both the systems was found to be very similar, the binding is governed by gain in enthalpy, which was found to be high for *c-MYC* compared to *c-KIT1* quadruplex DNA (Table 3).

Summary and Conclusions

In summary, we have synthesized a new series of benzothiazole hydrazone of furylbenzamide based potent G-quadruplex stabilizing ligands with different side chains and studied their interactions with various G-quadruplex and duplex DNAs. Based on the results from CD melting, FID assay and *Taq* DNA polymerase stop assay we conclude that all the ligands can preferentially stabilize the parallel topology of *c-MYC* and *c-KIT1* promoter G-quadruplex DNAs over antiparallel topology of *h-RAS1* promoter, various topologies of telomeric quadruplex and duplex DNAs. Among the three ligands studied, the ligand **2** with propyl side chain emerged as the most promising candidate. Molecular modeling and dynamics studies revealed that along with the π - π stacking of the aromatic units of the molecular scaffold with the G-quartet, the electrostatic interaction of the positively charged side chains play important role in stabilizing parallel quadruplex DNA topology of *c-MYC* and *c-KIT1* promoter DNAs. Overall, our studies show that preferential binding toward a particular G-quadruplex topology can be achieved with the help of suitably designed simple structural scaffolds, which satisfy desired criteria for small molecule drugs. Our current efforts are directed towards engineering these scaffolds to enhance the target specificity as well to screen their biological activities. It should be noted here that since RNA and some of the other promoter quadruplex DNAs can adopt parallel structures, it is indeed a challenging task to design ligands, which are capable to discriminate various parallel G-quadruplex topologies.

Experimental section

General. All the non-aqueous reactions were performed under nitrogen atmosphere using oven-dried glass wares. MeOH and DCM were dried using calcium hydride and commercially available DMF was dried by sequential incubation with molecular sieves under nitrogen atmosphere. Thin layer chromatography (TLC) was performed on silica gel 60 F₂₅₄ plates pre-coated with fluorescent indicator with visualization by UV light (254 nm). Silica gel (100-200 mesh) was used for column chromatography. ¹H NMR (400 MHz and 500 MHz), ¹³C NMR (100 MHz and 125 MHz) and ¹⁹F NMR (376 MHz and 470 MHz) were recorded on a 400 MHz and 500 MHz instruments. The chemical shifts in parts per million (δ) were reported downfield from TMS (0 ppm) and referenced to the TMS signal (0 ppm) or residual proton signal of deuterated solvents as follows: CDCl₃ (7.26 ppm), DMSO-*d*₆ (2.50 ppm) and CD₃OD (3.31 ppm) for ¹H NMR spectra; CDCl₃ (77.2 ppm), DMSO-*d*₆ (39.5 ppm) and CD₃OD (49.1 ppm) for ¹³C NMR spectra. Multiplicities of ¹H NMR spin couplings are reported as s (singlet), d (doublet), t (triplet), q (quartet), dd (doublet of doublets), dt (doublet of triplate), tt (triplet of triplet), br. s. (broad singlet) or m (multiplet and overlapping spin systems). Values for apparent coupling constants (*J*) are reported in Hz. High resolution mass spectras (HRMS) were obtained in positive ion electron spray ionization (ESI) mode using Q-TOF analyser.

Synthetic procedures

(Z)-2,3,5,6-tetrafluorophenyl-3-(5-(1-(2-(benzo[d]thiazol-2-yl)hydrazono)ethyl)furan-2-yl)benzoate (5). Compound **4** (500mg, 1.32 mmol) was dissolved in dry DMF (5 mL) with gentle heating. EDCI (504 mg, 2.64mmol) and 2,3,5,6-tetrafluorophenol (422 mg, 2.64 mmol) were added and the reaction was stirred at room temperature for 6 h. After completion of the reaction, DCM (3 × 50 mL) was added and the excess DMF and EDCI were removed by extraction with water (3 × 50 mL). The organic layer was dried over anhydrous Na₂SO₄,

evaporated under reduced pressure, and purified by column chromatography on silica gel using 20% ethyl acetate in petroleum ether to give the compound **5** as a yellow solid. Yield: 70% (501 mg); R_f = 0.3 (50% ethyl acetate in petroleum ether); mp = 189-192 °C. ^1H NMR (500 MHz, CDCl_3): δ 8.53 (t, J = 1.7 Hz, 1 H), 8.13 (dt, J = 7.9, 1.3 Hz, 1 H), 8.07 (dt, J = 7.9, 1.3 Hz, 1 H), 7.67 (d, J = 7.9 Hz, 1H), 7.62 (t, J = 7.8 Hz, 1H), 7.54 (d, J = 7.9 Hz, 1H), 7.34 (t, J = 7.5 Hz, 1H), 7.17 (t, J = 7.6 Hz, 1H), 7.07 (tt, J = 9.9, 7.0 Hz, 1H), 6.90 (q, J = 3.6 Hz, 2H), 2.31 (s, 3H). ^{13}C NMR (125 MHz, CDCl_3): δ 168.4, 162.3, 152.9, 152.1, 149.4, 147.4, 140.6, 131.1, 130.1, 129.8, 129.6, 129.4, 127.8, 126.0, 126.0, 122.3, 121.4, 118.2, 111.6, 108.7, 103.6, 103.4, 103.2, 12.8. ^{19}F NMR (470 MHz, CDCl_3): δ -138.7, -152.5 HRMS (ESI): calcd for $\text{C}_{26}\text{H}_{15}\text{F}_4\text{N}_3\text{O}_3\text{S}$, $[\text{M} + \text{Na}]^+$ 548.0662; found, $[\text{M} + \text{Na}]^+$ 548.0663 (Δm = -0.0001 and error = -0.1 ppm).

(Z)-3-(5-(1-(2-(benzo[d]thiazol-2-yl)hydrazono)ethyl)furan-2-yl)-N-Boc-carbamimidoylbenzamide (6). Compound **5** (150 mg, 0.27 mmol) was dissolved in DCM (2 mL) and *N*-Boc-guanidine (220 mg, 1.38mmol) was added followed by the addition of by adding MeOH (2 mL). The reaction mixture was stirred at room temperature for 6 h. After completion of the reaction, the solvent was evaporated and purified by column chromatography on silica using 30% ethyl acetate in petroleum ether to give the compound **6** as a yellow solid. Yield: 56% (77 mg); R_f = 0.5 (50% ethyl acetate in petroleum ether); mp = 205-210 °C. ^1H NMR (400 MHz, $\text{DMSO}-d_6$): δ 11.38 (s, 1H), 9.66 (br. s., 1H), 8.65 (br. s., 1H), 8.48 (s, 1H), 8.03 (d, J = 7.8 Hz, 1H), 7.92 (d, J = 7.5 Hz, 1H), 7.71 (d, J = 6.5 Hz, 1H), 7.55 (t, J = 7.8 Hz, 1H), 7.25-7.30 (m, 1H), 7.10 (d, J = 3.3 Hz, 1H), 7.07 (t, J = 7.6 Hz, 1H), 7.01 (d, J = 3.3 Hz, 1H), 2.33 (s, 3H), 1.48 (s, 9H). ^{13}C NMR (100 MHz, $\text{DMSO}-d_6$): δ 176.3, 167.8, 159.2, 154.6, 153.7, 152.3, 138.4, 130.1, 129.2, 128.5, 126.9, 126.4, 124.5, 122.2, 121.9, 112.6, 108.8, 82.9, 28.1, 14.3. HRMS (ESI): calcd for $\text{C}_{26}\text{H}_{26}\text{N}_6\text{O}_4\text{S}$, $[\text{M} + \text{Na}]^+$ 541.1628; found, $[\text{M} + \text{Na}]^+$ 541.1625 (Δm = +0.0003 and error = +0.6 ppm).

(Z)-3-(5-(1-(2-(benzo[d]thiazol-2-yl)hydrazono)ethyl)furan-2-yl)-N-(3-(dimethylamino)propyl)benzamide (7). Compound **5** (80 mg, 0.15 mmol) was dissolved in DCM (3 mL) and to which *N,N*-dimethyl-1,3-propanediamine (0.2 mL, 1.5 mmol) was added and the reaction mixture was stirred at room temperature for 3 h. After completion of the reaction, DCM (3 × 50 mL) was added and the excess amine was removed by extraction with water (3 × 50 mL). The organic layer was dried over anhydrous Na₂SO₄, concentrated to get an orange coloured solid compound **7**. Yield: 67% (47 mg); *R*_f = 0.6 (15% MeOH in DCM). ¹H NMR (400 MHz, CDCl₃): δ 8.56 (t, *J* = 4.4 Hz, 1H), 8.13 (br. s., 1H), 7.85 (d, *J* = 7.6 Hz, 1H), 7.63-7.67 (m, 2H), 7.44-7.49 (m, 2H), 7.30 (t, *J* = 7.5 Hz, 1H), 7.14 (t, *J* = 7.5 Hz, 1H), 6.86 (d, *J* = 3.4 Hz, 1H), 6.80 (d, *J* = 2.4 Hz, 1H), 3.6 (q, *J* = 5.7 Hz, 2H), 2.50-2.56 (m, 2H), 2.31 (s, 6H), 2.24 (s, 3H), 1.78-1.83 (m, 2H). ¹³C NMR (100 MHz, CDCl₃): δ 168.9, 167.2, 154.1, 152.1, 149.2, 141.7, 135.4, 130.9, 130.1, 129.2, 126.7, 126.3, 126.2, 123.1, 122.4, 121.7, 118.0, 111.8, 108.4, 58.6, 45.2, 40.1, 25.4, 13.3. HRMS (ESI): calcd for C₂₅H₂₇N₅O₂S, [M + Na]⁺ 484.1778; found, [M + Na]⁺ 484.1771 (Δ*m* = +0.0007 and error = +1.3 ppm).

(Z)-1-(3-(5-(1-(2-(benzo[d]thiazol-2-yl)hydrazono)ethyl)furan-2-yl)benzoyl)guanidinium 2,2,2-trifluoroacetate (ligand 1). Compound **6** (30 mg, 0.06 mmol) was dissolved in DCM (2 mL). To this, trifluoro acetic acid (0.05 mL, 0.6 mmol) was added and was allowed to stirred for 1 h. Then the solvent was evaporated and dried in high vacuum to remove the excess of trifluoro acetic acid. The crude product was dissolved in minimum amount of 1% MeOH in DCM then precipitated with the addition of petroleum ether (2 mL). The supernatant was decanted and the same precipitation procedure was repeated for 6-7 times to get pure yellow coloured solid. Yield: 98% (23.5 mg); *R*_f = 0.6 (20% MeOH in DCM); mp = 235-240 °C. ¹H NMR (400 MHz, DMSO-*d*₆): δ 11.59 (br. s., 1H), 8.66 (br. s., 2H), 8.43 (br. s., 2H), 8.29 (br. s., 1H), 8.09 (d, *J* = 7.8 Hz, 1H), 7.86 (d, *J* = 8.0 Hz, 1H), 7.67-7.73 (m, 2H), 7.27-7.32 (m, 2H), 7.24 (d, *J* = 3.5 Hz, 1H), 7.07 (t, *J* = 7.9 Hz, 1H), 7.03 (d, *J* = 3.5 Hz,

1H), 2.32 (br. s., 3H). ¹³C NMR (100 MHz, DMSO-*d*₆): δ 167.4, 158.7, 158.4, 158.0, 155.1, 152.4, 152.1, 132.6, 130.5, 129.7, 128.3, 127.1, 126.0, 123.1, 121.8, 121.5, 117.5, 114.6, 112.3, 109.5, 13.8. ¹⁹F NMR (376 MHz, DMSO-*d*₆): δ -74.4. HRMS (ESI): calcd for C₂₁H₁₉N₆O₂S, [M]⁺ 419.1285; found, [M]⁺ 419.1289 (Δ*m* = -0.0004 and error = -1.0 ppm).

(Z)-3-(3-(5-(1-(2-(benzo[d]thiazol-2-yl)hydrazono)ethyl)furan-2-yl)benzamido)-N,N-dimethylpropan-1-aminium 2,2,2-trifluoroacetate (ligand 2). Compound **7** (35 mg, 0.07mmol) was dissolved in DCM (2 mL). To this, trifluoro acetic acid (0.05 mL, 0.7mmol) was added and it was allowed to stir for 1 h. Then the solvent was evaporated and dried under high vacuum to remove the excess of trifluoro acetic acid. The crude mass was dissolved in minimum amount of 1% MeOH in DCM then precipitated with the addition of petroleum ether (2 mL) and finally the supernatant was decanted. The same precipitation procedure was repeated for 6-7 times to get pure yellow coloured sticky solid ligand **2**. Yield: 98% (14 mg); *R*_F = 0.6 (15% MeOH in DCM). ¹H NMR (500 MHz, CD₃OD): δ 8.23 (s, 1H), 7.91 (d, *J* = 7.9 Hz, 1H), 7.76 (d, *J* = 7.6 Hz, 1H), 7.70 (d, *J* = 7.6 Hz, 1H), 7.50 (t, *J* = 7.6 Hz, 1H), 7.45 (d, *J* = 7.9 Hz, 1H), 7.36 (t, *J* = 7.5 Hz, 1H), 7.20 (t, *J* = 7.5 Hz, 1H), 7.02 (d, *J* = 3.6 Hz, 1H), 6.96 (d, *J* = 3.4 Hz, 1H), 3.52 (t, *J* = 6.4 Hz, 2H), 3.20-3.24 (m, 2H), 2.92 (s, 6H), 2.35 (s, 3H), 2.07 (dt, *J* = 14.0, 6.7 Hz, 2H). ¹³C NMR (125 MHz, CD₃OD): δ 170.3, 169.7, 155.8, 152.8, 146.6, 144.7, 135.9, 132.0, 130.4, 128.2, 128.0, 127.8, 124.5, 124.2, 123.3, 119.1, 116.8, 114.8, 109.7, 56.8, 48.8, 37.7, 26.3, 14.0. ¹⁹F NMR (470 MHz, CD₃OD): δ -77.0. HRMS (ESI): calcd for C₂₅H₂₈N₅O₂S, [M]⁺ 462.1958; found, [M]⁺ 462.1962 (Δ*m* = -0.0004 and error = +0.9 ppm).

(Z)-3-(5-(1-(2-(benzo[d]thiazol-2-yl)hydrazono)ethyl)furan-2-yl)-N-(2-(dimethylamino)ethyl)benzamide (ligand 3). Compound **5** (170 mg, 0.32 mmol) was dissolved in DCM (5 mL) and *N,N*-dimethyl-1,2-ethanediamine (0.35 mL, 3.2mmol) was added and the reaction mixture was stirred at room temperature for 3 h. After completion of

the reaction, DCM ($3 \times 50\text{mL}$) was added and the excess amine was removed by extraction with water ($3 \times 50\text{mL}$). The organic layer was dried over anhydrous Na_2SO_4 , evaporated under reduced pressure to give the yellow coloured solid compound **3**. Yield: 70% (102 mg); $R_f = 0.5$ (15% MeOH in DCM); mp = 193-196 °C. ^1H NMR (500 MHz, CDCl_3): δ 8.14 (br. s., 1H), 7.83 (d, $J = 7.9$ Hz, 1H), 7.62 (t, $J = 6.4$ Hz, 2H), 7.40-7.46 (m, 2H), 7.30 (t, $J = 7.6$ Hz, 1H), 7.13 (t, $J = 7.6$ Hz, 1H), 6.83 (d, $J = 3.0$ Hz, 1H), 6.79 (d, $J = 2.7$ Hz, 1H), 3.60 (q, $J = 5.2$ Hz, 2H), 2.60 (t, $J = 5.8$ Hz, 2H), 2.30 (s, 6H), 2.27 (s, 3H). ^{13}C NMR (125 MHz, CDCl_3): δ 168.7, 167.6, 153.8, 151.8, 148.7, 141.5, 135.1, 130.7, 129.8, 129.0, 126.6, 126.1, 126.1, 122.9, 122.2, 121.5, 117.6, 111.6, 108.3, 58.1, 45.0, 37.1, 13.1. HRMS (ESI): calcd for $\text{C}_{24}\text{H}_{25}\text{N}_5\text{O}_2\text{S}$, $[\text{M} + \text{H}]^+$ 448.1802; found, $[\text{M} + \text{H}]^+$ 448.1805 ($\Delta m = +0.0003$ and error = +0.8 ppm).

Ligand stock solution. Stock solutions (5 mM) of all the ligands were made in DMSO. For ligand **3**, stock solution was further diluted to 1 mM using 10 mM HCl in water.

DNA oligonucleotides. The oligonucleotide sequences used for all the experiments are listed in Table S3 (Supporting Information). The oligonucleotides were synthesized in $1\mu\text{M}$ scale using Mermade-4 DNA synthesizer. After synthesis, oligonucleotides were deprotected and purified by 20% PAGE using standard protocols. Oligonucleotides used for the fluorimetric titration studies were commercially purchased and purified by 20% PAGE. The concentration of all DNAs was calculated at 260 nm in the Perkin Elmer Lambda Bio⁺ UV spectrophotometer using appropriate molar extinction coefficients (ϵ).

CD titration studies. CD titration experiments were performed using Jasco 815 CD spectrometer. All the CD spectras were recorded at the wavelength range of 220-320 nm using 1 mm path length quartz cuvette. The scanning speed was 100 nm/min with a response time of 2 sec at 25 °C. The strand concentration of DNA was $12.5\mu\text{M}$ in 50 mM of Tris-HCl buffer, pH 7.2. Initially, the baseline was recorded with 50 mM Tris-HCl buffer, pH 7.2,

which was used for baseline subtraction. After each addition of the ligand (1 eq each) to DNA, solution was thoroughly mixed and kept for 5 minutes to attain equilibrium. Each spectrum was taken as an average of 3 measurements and analysed by using Origin 8.0 software.

CD melting studies. All the melting experiments were performed using Jasco 815 CD spectrometer. For melting studies, 10 μM strand concentration of quadruplex and 15 μM duplex DNAs in 10 mM lithium cacodylate, pH 7.2 or sodium cacodylate, pH 7.2, required amount of monovalent salts (KCl or NaCl and LiCl), and 5 molar equivalents of ligands (50-75 μM) were used. Telomeric DNA in K^+ ions (10 mM KCl and 90 mM LiCl), telomeric DNA in Na^+ ion (20 mM NaCl and 80 mM LiCl), *c-KIT1* DNA (10 mM KCl and 90 mM LiCl), *c-MYC* DNA (1 mM KCl and 99 mM LiCl), *h-RAS1* DNA (50 mM KCl and 50 mM LiCl) and duplex DNA (10 mM KCl and 90 mM LiCl) were annealed by heating at 95 $^{\circ}\text{C}$ for 5 min, followed by gradual cooling to room temperature over 3-4 h. Ligands (5 equivalents) were added to the annealed DNAs and kept at 4 $^{\circ}\text{C}$ for overnight. Thermal melting was monitored at 295, 290, 263, and 242 nm for telomeric, *h-RAS1*, promoter, and duplex DNAs respectively, at a heating rate of 1 $^{\circ}\text{C}/\text{min}$. The melting temperatures were determined from sigmoidal curve fit using the Boltzmann function in Origin 8.0 software.

Fluorescence intercalator displacement assay. FID assay was performed using Cary Eclipse spectrofluorimeter using 1 mL quartz cuvette having 1 cm path length. The quadruplex and duplex DNA (0.25 μM) in 100 mM KCl and 10 mM lithium cacodylate buffer, pH 7.2 were annealed by heating at 95 $^{\circ}\text{C}$ for 5 minute followed by slow cooling to room temperature for 3-4 h. To the annealed quadruplex DNA, 0.50 μM and to the duplex DNA, 0.75 μM of Thiazole Orange dye was added and allowed to equilibrate for 2 h at 4 $^{\circ}\text{C}$. The emission spectrum was recorded in the range of 505-700 nm with an excitation wavelength of 500 nm with a slit width of 5 nm. Ligand (0-30 μM) was added to the DNA-TO complex and

emission spectra were recorded for each addition after 3 minutes equilibration. The fluorescence area under each curve was calculated and further converted to the percentage of TO displacement value using the equation,

$$\text{Percentage of TO displacement} = 100 - \left[\left(\frac{F}{F_0} \right) \times 100 \right]$$

Where F_0 = fluorescence area without ligand, F = fluorescence area in presence of ligand. The percentage of TO displacement was plotted against the concentration of ligands and the DC_{50} values were determined. All spectra were analysed by origin 8.0 software.

Fluorimetric titration studies. Fluorimetric titration experiments were performed using Cary Eclipse spectrofluorimeter using 1 mL quartz cuvette having 1 cm path length. Quadruplex and duplex DNAs (5 μ M) in 100 mM KCl and 10 mM lithium cacodylate buffer, pH 7.2 were annealed by heating at 95 $^{\circ}$ C for 5 minutes followed by gradual cooling to room temperature for 3-4 h. The DNAs were excited at an excitation wavelength of 367 nm and the emission spectra was recorded in the range of 372-700 nm using a slit width of 5 nm. Ligand **2** (0- 24 μ M for c-MYC DNA and 0-50 μ M for telomeric and duplex DNAs) was titrated to the DNA sample and the emission spectra was recorded after an equilibration for 3 minutes. A spectral blank was measured with only ligand **2** in buffer and the corresponding fluorescence intensity was deducted from the original intensities of ligand **2** with DNA. Normalised fluorescence intensity (F_N) was plotted against the logarithm of concentration of the ligand and the following equation (Hill1 equation) was used for curve fitting to derive the apparent binding constant (K_d) values.

$$F_N = F_0 + (F_S - F_0) \left(\frac{[L]^n}{[K_d]^n + [L]^n} \right)$$

Normalised fluorescence intensity (F_N) was derived using the equation,

$$F_N = \frac{(F_i - F_0)}{(F_S - F_0)}$$

Where F_i = fluorescence intensity of bound ligand at each titration point, F_0 = fluorescence intensity in the absence of ligand, and F_s = fluorescence intensity at the saturation concentration of ligand. L = concentration of ligand, n = Hill coefficient i.e., the degree of cooperative binding, K_d = dissociation constant ($1/K_a$). All the experiments were triplicated and the spectras were analysed by Origin 8.0 software.

5'-end labelling. 5'-end of the DNA primer(10 pmol) was labelled with [γ^{32} -P] ATP (10 μ Ci) by using T4 polynucleotide kinase (PNK, 5 U) in $1 \times$ PNK buffer (50 mM Tris-HCl, pH 7.6, 10 mM $MgCl_2$, 5 mM DTT, 0.1 mM spermidine and 0.1 mM EDTA). Total volume of the reaction mixture was maintained 10 μ L. The reaction mixture was incubated for at 37 °C for 1 h for forward reaction, and the enzyme activity was stopped by heating at 70 °C for 3 minutes. Labelled DNA was purified by using QIA quick nucleotide removal kit using the protocol provided by the manufacturer.

Taq DNA polymerase stop assay. Appropriate amount of radiolabelled primer, unlabelled primer(50 nM) and template (100 nM) in buffer (5 mM Tris-HCl, pH 8.0, 15 mM NaCl, 0.1mM EDTA) were annealed by heating at 95 °C for 5 minutes followed by gradual cooling to room temperature for 3-4 h. The annealed primer-template DNA was mixed with $1 \times$ polymerase buffer (50 mM Tris-HCl, pH 8.0, 0.5 mM DTT, 0.1 mM EDTA, 5 mM $MgCl_2$, 5mM KCl for *c-MYC* and 10 mM KCl for telomeric DNA template), 1 μ g/ μ L BSA in 5% glycerol and 0.2mM dNTPs. Appropriate amount of ligands (0-50 μ M for *c-MYC* and 0-200 μ M for telomeric and mutated DNAs) were added in a total volume of 10 μ L and the reaction mixture was incubated for 30 minutes at room temperature. *Taq* DNA polymerase enzyme (0.5 U) was added to initiate the primer extension reaction, and heated at 55 °C for *c-MYC* and 40 °C for telomeric DNA template for 30 minutes. After completion of reaction, the extension reaction was stopped by adding 10 μ L of $2 \times$ stop dye (80% formamide, $1 \times$ TBE, 50 mM EDTA, pH 8.0, 0.025% each bromophenolblue and xylene cyanole FF) to the

reaction mixture and the DNA was denatured at 95 °C for 3 minutes. The extension products were analysed by 15 % denaturing PAGE (7 M urea) in 1 × TBE (89 mM of Tris-HCl and boric acid each, 2 mM EDTA, pH 8.2) running buffer. The gels were kept inside the cassette for 2h and analysed by autoradiography using a phosphorimager. The bands were quantified by using Image Quant 5.2 software and the the percentage of stop product was plotted against the concentration of ligands using Origin 8.0 software to derive the IC₅₀ values.

Molecular modeling and dynamics study. The ligand **2** was optimized in Gaussian09⁵⁸ in different stages. First step of optimization at a low theoretical level (PM3), which was followed by optimization at a finer theoretical level (HF/6-311+G**). Final step involved the rotation of N2-N1 bond to orient the benzothiazole moiety in the plane of ligand, and then the ligand is optimized at a theoretical level HF/6-311+G** to obtain the final structure (Fig S8, Supporting Information). Optimized ligand **2** was docked with *c-MYC* (PDB entry: 2L7V) and *c-KIT1* (PDB entry: 2O3M) DNAs using the Lamarckian genetic algorithm in AutoDock 4.2⁵² to generate 250 independent docked conformations. Ligands were removed from *c-MYC* PDB file (2L7V) and the 5' end residue dA was removed from the *c-KIT1* PDB file (2O3M) to facilitate the docking. Also, the nitrogen atom on the propyl side chain of the ligand **2** was protonated to explore the electrostatic interactions. A restricted grid docking was carried out to explore the conformational space available at the 5'end of *c-KIT1*, whereas whole DNA was considered in case of *c-MYC*. The generalized amber force field (GAFF)⁵⁹ and ff09bsc0⁶⁰ force fields were used for the ligand and the DNA respectively. RESP⁶¹ charge fitting was done using antechamber⁶² of AMBER 14. The system was solvated using TIP3P water molecules extending up to 10 Å in a truncated octahedron. K⁺ ions were added to neutralize the system. The solvated system was subjected to 10000 steps of minimization, 100 ps of heating with restriction on ligand, 100 ps of density equilibration and 800ps of final equilibration followed by 500 ns of unrestrained dynamics with coordinates saved every 2ps.

The time step for dynamics was 2 fs and the temperature was maintained at 300 K using Langevin thermostat. The dynamics was run using GPU accelerated implementation of PMEMD in AMBER 14.⁵³⁻⁵⁶ Binding free energies were estimated using MM-PBSA⁵⁷ (MMPBSA.py) method over last 20 ns. Every 5th frame was considered, and a total of 2000 frames were considered for binding energy calculations. RMSDs of the heavy atoms, Hoogsteen bond occupancies and distances were calculated for every 10 ps (every 5th frame using CPPTRAJ and PTRAJ⁶³ modules. A cut off value of 3.5 Å between heavy atoms is considered for defining H-bond and cut off value of 3.5 Å is considered for defining electrostatic interactions. Cut off values of 5 Å between centroids of aromatic rings and an angle of 20° between planes of aromatic rings were considered for defining stacking interactions. RMSF values were calculated residue wise for every 5th frame and a total of 50,000 frames were considered. Every 25th frame (every 50 ps) was considered for calculation of stacking distances and angles. UCSFChimera⁶⁴ was used for the visualization of MD simulations, calculation of stacking distances and angles. PyMOL (<http://www.pymol.org>) was used for rendering images.

Acknowledgements

We are thankful to the financial support from Department of Biotechnology (DBT), Government of India (Pilot Project Grants for Young Investigators in Cancer Biology, Grant No: 6242-P4/RGCB/PMD/DBT/PKPI/2015) and IRCC IIT Bombay. We thank Professor Ruchi Anand and Professor Krishna P. Kaliappan for providing access to their laboratory facilities. We are grateful to the central facility supported by IRCC-IIT Bombay for MALDI spectra, and the computer centre, IIT Bombay, for the the HPC facility. We also thank Ashil S. for his support in the synthesis of ligands, and S. Harikrishna and Ruhee D'cunha for their suggestions and assistance in molecular modeling studies. S.P.P and K.V.D. thank Council of Scientific and Industrial Research (CSIR), Government of India for Ph. D. fellowships, and

P.B. thank Department of Science and Technology (DST), Government of India for the INSPIRE fellowship.

References

1. G. W. Collie and G. N. Parkinson, *Chem. Soc. Rev.*, 2011, **40**, 5867-5892.
2. S. M. Haider, S. Neidle and G. N. Parkinson, *Biochimie*, 2011, **93**, 1239-1251.
3. M. L. Bochman, K. Paeschke and V. A. Zakian, *Nat. Rev. Genet.*, 2012, **13**, 770-780.
4. N. Maizels and L. T. Gray, *PLoS Genet.*, 2013, **9**, e1003468.
5. J. L. Huppert and S. Balasubramanian, *Nucleic Acids Res.*, 2007, **35**, 406-413.
6. G. Biffi, D. Tannahill, J. McCafferty and S. Balasubramanian, *Nat. Chem.*, 2013, **5**, 182-186.
7. A. Shivalingam, M. A. Izquierdo, A. L. Marois, A. Vysniauskas, K. Suhling, M. K. Kuimova and R. Vilar, *Nat. Commun.*, 2015, **6**, 8178.
8. A. Henderson, Y. Wu, Y. C. Huang, E. A. Chavez, J. Platt, F. B. Johnson, R. M. Brosh, D. Sen and P. M. Lansdorp, *Nucleic Acids Res.*, 2014, **42**, 860-869.
9. S. Burge, G. N. Parkinson, P. Hazel, A. K. Todd and S. Neidle, *Nucleic Acids Res.*, 2006, **34**, 5402-5415.
10. N. An, A. M. Fleming, E. G. Middleton and C. J. Burrows, *Proc. Natl. Acad. Sci.*, 2014, **111**, 14325-14331.
11. Y. Chen and D. Yang, *Curr. Protoc. Nucleic Acid Chem.*, 2012, **50**, 17.15.11-17.15.17.
12. A. T. Phan, Y. S. Modi and D. J. Patel, *J. Am. Chem. Soc.*, 2004, **126**, 8710-8716.
13. A. M. Zahler, J. R. Williamson, T. R. Cech and D. M. Prescott, *Nature*, 1991, **350**, 718-720.
14. S. Balasubramanian, L. H. Hurley and S. Neidle, *Nat. Rev. Drug discovery*, 2011, **10**, 261-275.

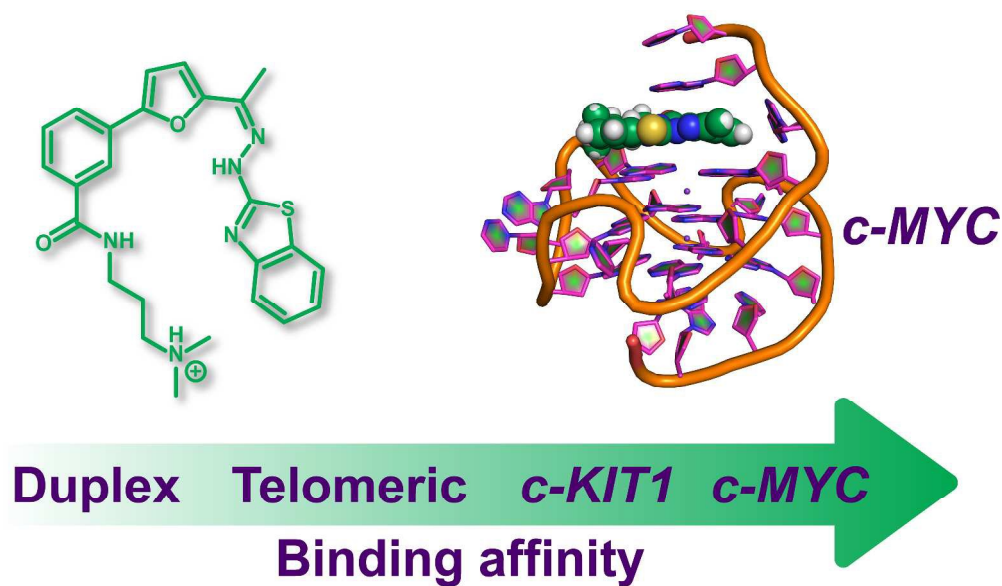
15. D. Rhodes and H. J. Lipps, *Nucleic Acids Res.*, 2015, **43**, 8627-8637.
16. J. Bidzinska, G. Cimino-Reale, N. Zaffaroni and M. Folini, *Molecules*, 2013, **18**, 12368-12395.
17. S. A. Ohnmacht and S. Neidle, *Bioorg. Med. Chem. Lett.*, 2014, **24**, 2602-2612.
18. D. Monchaud and M. P. Teulade-Fichou, *Org. Biomol. Chem.*, 2008, **6**, 627-636.
19. S. Neidle, *J. Med. Chem.*, 2016, DOI: 10.1021/acs.jmedchem.5b01835.
20. S. Zhang, Y. Wu and W. Zhang, *ChemMedChem*, 2014, **9**, 899-911.
21. M.Y. Kim, H. Vankayalapati, K. Shin-ya, K. Wierzba and L. H. Hurley, *J. Am. Chem. Soc.*, 2002, **124**, 2098-2099.
22. J. Dash, P. S. Shirude, S.-T. D. Hsu and S. Balasubramanian, *J. Am. Chem. Soc.*, 2008, **130**, 15950-15956.
23. V. Dhamodharan, S. Harikrishna, C. Jagadeeswaran, K. Halder and P. I. Pradeepkumar, *J. Org. Chem.*, 2012, **77**, 229-242.
24. W. J. Chen, C. X. Zhou, P. F. Yao, X. X. Wang, J. H. Tan, D. Li, T. M. Ou, L. Q. Gu and Z. S. Huang, *Bioorg. Med. Chem.*, 2012, **20**, 2829-2836.
25. A. Altieri, A. Alvino, S. Ohnmacht, G. Ortaggi, S. Neidle, D. Nocioni, M. Franceschin and A. Bianco, *Molecules*, 2013, **18**, 13446-13470.
26. P. V. Boddupally, S. Hahn, C. Beman, B. De, T. A. Brooks, V. Gokhale and L. H. Hurley, *J. Med. Chem.*, 2012, **55**, 6076-6086.
27. R. V. Brown, F. L. Danford, V. Gokhale, L. H. Hurley and T. A. Brooks, *J. Biol. Chem.*, 2011, **286**, 41018-41027.
28. Y. Ma, T. M. Ou, J. H. Tan, J. Q. Hou, S. L. Huang, L. Q. Gu and Z. S. Huang, *Eur. J. Med. Chem.*, 2011, **46**, 1906-1913.
29. D. Peng, J. H. Tan, S. B. Chen, T. M. Ou, L. Q. Gu and Z. S. Huang, *Bioorg. Med. Chem.*, 2010, **18**, 8235-8242.

30. T. Agarwal, S. Roy, T. K. Chakraborty and S. Maiti, *Biochemistry*, 2010, **49**, 8388-8397.
31. K. V. Diveshkumar, S. Sakrikar, S. Harikrishna, V. Dhamodharan and P. I. Pradeepkumar, *ChemMedChem*, 2014, **9**, 2754-2765.
32. V. Dhamodharan, S. Harikrishna, A. C. Bhasikuttan and P. I. Pradeepkumar, *ACS Chem. Biol.*, 2015, **10**, 821-833.
33. A. Chauhan, S. Paladhi, M. Debnath, S. Mandal, R. N. Das, S. Bhowmik and J. Dash, *Bioorg. Med. Chem.*, 2014, **22**, 4422-4429.
34. K. M. Felsenstein, L. B. Saunders, J. K. Simmons, E. Leon, D. R. Calabrese, S. Zhang, A. Michalowski, P. Gareiss, B. A. Mock and J. S. Schneekloth, *ACS Chem. Biol.*, 2016, **11**, 139-148.
35. G. Lessene, P. E. Czabotar, B. E. Sleebs, K. Zobel, K. N. Lowes, J. M. Adams, J. B. Baell, P. M. Colman, K. Deshayes, W. J. Fairbrother, J. A. Flygare, P. Gibbons, W. J. A. Kersten, S. Kulasegaram, R. M. Moss, J. P. Parisot, B. J. Smith, I. P. Street, H. Yang, D. C. S. Huang and K. G. Watson, *Nat. Chem. Biol.*, 2013, **9**, 390-397.
36. M. Yoshida, I. Hayakawa, N. Hayashi, T. Agatsuma, Y. Oda, F. Tanzawa, S. Iwasaki, K. Koyama, H. Furukawa, S. Kurakata and Y. Sugano, *Bioorg. Med. Chem. Lett.*, 2005, **15**, 3328-3332.
37. S. Chandrappa, C. V. Kavitha, M. S. Shahabuddin, K. Vinaya, C. S. Ananda Kumar, S. R. Ranganatha, S. C. Raghavan and K. S. Rangappa, *Bioorg. Med. Chem.*, 2009, **17**, 2576-2584.
38. B. S. Holla, B. S. Rao, B. K. Sarojini and P. M. Akberali, *Eur. J. Med. Chem.*, 2004, **39**, 777-783.
39. B. E. Sleebs, W. J. A. Kersten, S. Kulasegaram, G. Nikolakopoulos, E. Hatzis, R. M. Moss, J. P. Parisot, H. Yang, P. E. Czabotar, W. D. Fairlie, E. F. Lee, J. M. Adams, L.

- Chen, M. F. van Delft, K. N. Lowes, A. Wei, D. C. S. Huang, P. M. Colman, I. P. Street, J. B. Baell, K. Watson and G. Lessene, *J. Med. Chem.*, 2013, **56**, 5514-5540.
40. M. K. Smalley and S. K. Silverman, *Nucleic Acids Res.*, 2006, **34**, 152-166.
41. A. Randazzo, G. Spada and M. W. Silva, *Top. Curr. Chem.*, 2013, **330**, 67-86.
42. A. Membrino, S. Cogoi, E. B. Pedersen and L. E. Xodo, *PLoS One*, 2011, **6**, e24421.
43. A. Guedin, L. Lacroix and J. L. Mergny, *Methods Mol. Biol.*, 2010, **613**, 25-35.
44. Y. Wang and D. J. Patel, *Structure*, 1993, **1**, 263-282.
45. D. Monchaud, C. Allain, H. Bertrand, N. Smargiasso, F. Rosu, V. Gabelica, A. De Cian, J. L. Mergny and M. P. Teulade-Fichou, *Biochimie*, 2008, **90**, 1207-1223.
46. S. G. Srivatsan and Y. Tor, *J. Am. Chem. Soc.*, 2007, **129**, 2044-2053.
47. A. A. Tanpure and S. G. Srivatsan, *Nucleic Acids Res.*, 2015, DOI: 10.1093/nar/gkv743.
48. H. Han, L. H. Hurley and M. Salazar, *Nucleic Acids Res.*, 1999, **27**, 537-542.
49. D. Sun and L. H. Hurley, *Methods Mol. Biol.*, 2010, **608**, 65-79.
50. J. Dai, M. Carver, L. H. Hurley and D. Yang, *J. Am. Chem. Soc.*, 2011, **133**, 17673-17680.
51. A. T. Phan, V. Kuryavyi, S. Burge, S. Neidle and D. J. Patel, *J. Am. Chem. Soc.*, 2007, **129**, 4386-4392.
52. G. M. Morris, D. S. Goodsell, R. S. Halliday, R. Huey, W. E. Hart, R. K. Belew and A. J. Olson, *J. Comput. Chem.*, 1998, **19**, 1639-1662.
53. R. Salomon-Ferrer, A. W. Götz, D. Poole, S. Le Grand and R. C. Walker, *J. Chem. Theory Comput.*, 2013, **9**, 3878-3888.
54. A. W. Götz, M. J. Williamson, D. Xu, D. Poole, S. Le Grand and R. C. Walker, *J. Chem. Theory Comput.*, 2012, **8**, 1542-1555.

55. S. Le Grand, A. W. Götz and R. C. Walker, *Comput. Phys. Commun.*, 2013, **184**, 374-380.
56. D. A. Case, T. A. Darden, T. E. Cheatham, C. L. Simmerling, J. Wang, R. E. Duke, R. Luo, R. C. Walker, W. Zhang, K. M. Merz, B. Roberts, B. Wang, S. Hayik, A. Roitberg, G. Seabra, I. Kolossváry, K. F. Wong, F. Paesani, J. Vanicek, J. Liu, X. Wu, S. R. Brozell, T. Steinbrecher, H. Gohlke, Q. Cai, X. Ye, J. Wang, M. J. Hsieh, G. Cui, D. R. Roe, D. H. Mathews, M. G. Seetin, C. Sagui, V. Babin, S. Gusarov, A. Kovalenko and P. A. Kollman, *AMBER 14*, University of California, San Francisco, CA (USA), 2014.
57. P. A. Kollman, I. Massova, C. Reyes, B. Kuhn, S. Huo, L. Chong, M. Lee, T. Lee, Y. Duan, W. Wang, O. Donini, P. Cieplak, J. Srinivasan, D. A. Case and T. E. Cheatham, *Acc. Chem. Res.*, 2000, **33**, 889-897.
58. M. J. Frisch, G. W. Trucks, H. B. Schlegel, G. E. Scuseria, M. A. Robb, J. R. Cheeseman, G. Scalmani, V. Barone, B. Mennucci, G. A. Petersson, H. Nakatsuji, M. Caricato, X. Li, H. P. Hratchian, A. F. Izmaylov, J. Bloino, G. Zheng, J. L. Sonnenberg, M. Hada, M. Ehara, K. Toyota, R. Fukuda, J. Hasegawa, M. Ishida, T. Nakajima, Y. Honda, O. Kitao, H. Nakai, T. Vreven, J. A. Montgomery Jr., J. E. Peralta, F. Ogliaro, M. J. Bearpark, J. Heyd, E. N. Brothers, K. N. Kudin, V. N. Staroverov, R. Kobayashi, J. Normand, K. Raghavachari, A. P. Rendell, J. C. Burant, S. S. Iyengar, J. Tomasi, M. Cossi, N. Rega, N. J. Millam, M. Klene, J. E. Knox, J. B. Cross, V. Bakken, C. Adamo, J. Jaramillo, R. Gomperts, R. E. Stratmann, O. Yazyev, A. J. Austin, R. Cammi, C. Pomelli, J. W. Ochterski, R. L. Martin, K. Morokuma, V. G. Zakrzewski, G. A. Voth, P. Salvador, J. J. Dannenberg, S. Dapprich, A. D. Daniels, Ö. Farkas, J. B. Foresman, J. V. Ortiz, J. Cioslowski and D. J. Fox, *Gaussian 09, Revision A. 02*, Gaussian Inc., Wallingford, CT (USA), 2009.

59. J. Wang, R. M. Wolf, J. W. Caldwell, P. A. Kollman and D. A. Case, *J. Comput. Chem.*, 2004, **25**, 1157-1174.
60. M. Zgarbová, M. Otyepka, J. Šponer, A. Mládek, P. Banáš, T. E. Cheatham and P. Jurečka, *J. Chem. Theory Comput.*, 2011, **7**, 2886-2902.
61. T. Fox and P. A. Kollman, *J. Phys. Chem. B*, 1998, **102**, 8070-8079.
62. J. Wang, W. Wang, P. A. Kollman and D. A. Case, *J. Mol. Graphics Model.*, 2006, **25**, 247-260.
63. D. R. Roe and T. E. Cheatham, *J. Chem. Theory Comput.*, 2013, **9**, 3084-3095.
64. E. F. Pettersen, T. D. Goddard, C. C. Huang, G. S. Couch, D. M. Greenblatt, E. C. Meng and T. E. Ferrin, *J. Comput. Chem.*, 2004, **25**, 1605-1612.



431x252mm (300 x 300 DPI)